Geophys. J. Int. (2002) **149,** 267–280

Processing, modelling and predicting time-lapse effects of overpressured fluid-injection in a fractured reservoir

Erika Angerer,[1,*] Stuart Crampin,[1,2] Xiang-Yang Li[2] and Thomas L. Davis[3]

[1]*Department of Geology and Geophysics, University of Edinburgh, Grant Institute, West Mains Road, Edinburgh* EH9 3JW, *UK.*
E-mails: erika.angerer@westerngeco.com; scrampin@ed.ac.uk
[2]*Edinburgh Anisotropy Project, British Geological Survey, Murchison House, West Mains Road, Edinburgh* EH9 3LA, *UK. E-mail: x.y.li@bgs.ac.uk*
[3]*Reservoir Characterization Project, Colorado School of Mines, Golden,* CO 80401, *USA*

Accepted 2001 September 11. Received 2001 September 7; in original form 2001 May 22

SUMMARY

Time-lapse seismology is important for monitoring subsurface pressure changes and fluid movements in producing hydrocarbon reservoirs. We analyse two 4-D, 3C onshore surveys from Vacuum Field, New Mexico, USA, where the reservoir of interest is a fractured dolomite. In Phase VI, a time-lapse survey was acquired before and after a pilot tertiary-recovery programme of overpressured CO_2 injection, which altered the fluid composition and the pore-fluid pressure. Phase VII was a similar time-lapse survey in the same location but with a different lower-pressure injection regime.

Applying a processing sequence to the Phase VI data preserving normal-incidence shear-wave anisotropy (time-delays and polarization) and maximizing repeatability, interval-time analysis of the reservoir interval shows a significant 10 per cent change in shear-wave velocity anisotropy and 3 per cent decrease in the *P*-wave interval velocities. A 1-D model incorporating both saturation and pressure changes is matched to the data. The saturation changes have little effect on the seismic velocities. There are two main causes of the time-lapse changes. Any change in pore-fluid pressures modifies crack aspect ratios. Additionally, when there are overpressures, as there are in Phase VI, there is a 90° change in maximum impedance directions, and the leading faster split shear wave, instead of being parallel to the crack face as it is for low pore-fluid pressures, becomes orthogonal to the crack face. The anisotropic poro-elasticity (APE) model of the evolution of microcracked rock, calculates the evolution of cracked rock to changing conditions. APE modelling shows that at high overburden pressures only nearly vertical cracks, to which normal incidence *P* waves are less sensitive than *S* waves, remain open as the pore-fluid pressure increases. APE modelling matches the observed time-lapse effects almost exactly demonstrating that shear-wave anisotropy is a highly sensitive diagnostic of pore-fluid pressure changes in fractured reservoirs.

In this comparatively limited analysis, APE modelling of fluid-injection at known pressure correctly *predicted* the changes in seismic response, particularly the shear-wave splitting, induced by the high-pressure CO_2 injection. In the Phase VII survey, APE modelling also successfully predicted the response to the lower-pressure injection using the same Phase VI model of the cracked reservoir. The underlying reason for this remarkable predictability of fluid-saturated reservoir rocks is the critical nature and high crack density of the fluid-saturated cracks and microcracks in the reservoir rock, which makes cracked reservoirs critical systems.

Key words: anisotropic poro-elasticity (APE), critical systems, fluid-injection, fractured reservoirs.

1 INTRODUCTION

The multicomponent 4-D (time-lapse 3-D) 3C reflection survey in Vacuum Field, New Mexico, in 1995, by the Reservoir Characterization Project (RCP), Colorado School of Mines, was the first time-lapse shear-wave acquisition in exploration seismology (Roche *et al.* 1997). Time-lapse seismology aims to record fluid movements within the reservoir, which may indicate, for example, isolated fluid compartments. Jack (1998) suggests that such integrated geological, geophysical and petroleum engineering methods are needed to create a well-resolved picture of a producing reservoir.

*Now at: WesternGeco, Schlumberger House, Gatwick Airport, West Sussex, RH6 0NZ, UK.

A large number of investigations of shear-wave propagation have shown the sensitivity of shear-wave splitting (seismic birefringence) to the presence of aligned microcracks and fractures, rendering the rock effectively anisotropic. Shear-wave anisotropy with azimuthal variations has been observed, for example, in laboratory studies (Rai & Hanson 1988; Duerrast & Siegesmund 1999), earthquake seismology (Liu *et al.* 1997; Crampin *et al.* 1999), and exploration seismology (Winterstein & Meadows 1991; Li & Crampin 1993; Thomsen *et al.* 1995; Gaiser 1999). Crampin (1994) reviewed all published observations of shear-wave splitting and showed that virtually all sedimentary, igneous and metamorphic rocks below about 1 km depth display shear-wave splitting with the polarization of the faster aligned subparallel to the direction of maximum horizontal compressional stress. That is, the faster shear waves are subparallel to the strike of stress-aligned cracks. Thus, the dominant fracture direction and the crack density can be estimated from the polarization directions and time-delays of the split shear waves. It is now generally accepted that crack directions are related to the subsurface stress directions, where open cracks are subparallel to the maximum horizontal stress.

Zatsepin & Crampin (1997) and Crampin & Zatsepin (1997) develop an anisotropic poro-elasticity (APE) model for the evolution of fluid-saturated cracks under changing conditions, particularly changes in subsurface stress. APE calculates the pressure- and stress-dependent distribution of microcracks, where the driving mechanism is fluid migration by flow or dispersion along pressure gradients between cracks at different orientations to the stress field. This causes compliant cracks to open and close dynamically and hence modifies the effective elastic constants of the fluid-filled rock, so that the changes can be monitored by shear-wave splitting. Crampin & Zatsepin (1997) show that changes in shear-wave splitting are controlled by exactly the same parameters that control low-level deformation before fracturing occurs.

The objective of this present study is: (1) process the Vacuum Field surface seismic data so that they can be reliably used for anisotropic time-lapse investigations; (2) analyse and identify anisotropic time-lapse effects; (3) calculate synthetic seismograms using APE for models that incorporate subsurface pressure and saturation changes from mixing the highly compressible CO_2 with the reservoir fluid for both Phase VI and Phase VII injection data sets. We shall see that the match of modelled to observed seismograms is so satisfactory that the response of the rock mass to known fluid-injection changes is in effect predicted. We shall suggest in an Appendix that this remarkable predictability of fluid–rock interactions is caused by the rock being so pervaded by cracks, in particular, fluid-saturated microcracks, that the rocks may be considered to be critical systems. This has several important implications for exploration and production geophysics as well as for a wide range of other earth science activities.

This study (Angerer *et al.* 2000a,b) shows the importance of shear-wave splitting as a time-lapse attribute in fractured reservoirs. We show that it is the principal seismic diagnostic for the detection of pressure effects, where even hard brittle rocks, such as dolomite, are suitable for time-lapse seismology. The modelling study is a verification and calibration of APE for surface seismic data.

2 OUTLINE OF PHASE VI

Vacuum Field is situated in the Permian Basin in New Mexico, USA. The reservoir interval of interest, the San Andres dolomite, is part of a flat-layered carbonate platform with cyclic deposition, which is overlain by evaporites and sandstones. Evidence of fracturing can be seen in cores and thin sections (Scuta 1997). Hydrocarbons have been produced for over 60 years making Vacuum Field a mature reservoir, which is now undergoing tertiary recovery in the form of CO_2 injections. We first analyse a pilot project in 1995, RCP Phase VI, where CO_2 was injected in a single well, CVU-97, for 3 weeks with a large increase in pore-fluid pressure. Two circular spread multicomponent surveys centred at CVU-97 were recorded before and immediately after the injection using *P*-wave and two shear-wave vibrator sources with orthogonal orientation and recorded by three-component receiver arrays. The 'nine-component' acquisition geometry is shown in Fig. 1 with the source lines oriented E–W and the receiver lines oriented N–S. Each source location has three sources and each receiver station also has three orthogonal components and therefore in total nine components are recorded per location. This allows one to sample the elastic wavefield with azimuth and offset. However, owing to insufficient quality the analysis was limited to normal move-out-stacked (NMO) data. The data analysis interval times and time-delays are evaluated from picked horizons, so that the shear-wave velocity anisotropy and *P*-interval velocity can be calculated. Shear-wave anisotropy is found to be the most sensitive parameter and a significant shear-wave splitting time-delay anomaly develops south and east of the injection well (Davis *et al.* 1997). Polarization directions are evaluated for the overburden and the target interval after layer-stripping following a method developed by Winterstein & Meadows (1991) and Thomsen *et al.* (1995).

In flat-layer modelling, we select a location in the zone of the shear-wave time-delay anomalies. The aim is to match the observed pre-injection data with synthetic seismograms propagating through an elastic model of aligned cracks. The synthetic seismograms were calculated using ANISEIS (Taylor 2000) which is a full waveform, anisotropic modelling package using the reflectivity method. Moreover, ANISEIS incorporates APE modelling. The modelling of the injection is separated into two parts: first, the evaluation of the effects of the saturation change; and second, the evaluation of the pore-fluid pressure changes. The change of the elastic parameters of the reservoir rock owing to CO_2 injection is calculated using inclusion models based on those developed by Endres & Knight (1997) to allow for the pore-fluid pressure communication at seismic frequencies. Pressure-dependent CO_2 properties have been determined experimentally by Wang *et al.* (1998). The resulting isotropic rock properties are the starting point for the pressure modelling.

Pressure changes are considered for an initial APE model of a cracked rock that was adapted to fit the observations of shear waves and *P* waves at the selected location. The measured pore-fluid pressure increase of 6.4 MPa causes previously closed nearly vertical low aspect-ratio cracks to open (increase in aspect ratio) during injection. The presence of fault zones also suggests preferred crack directions. All the seismic velocities decrease, particularly the shear waves with polarizations parallel to the maximum horizontal stress direction. This causes the observed change in anisotropy and, in particular *changes the polarization direction of the faster split shear wave*. APE shows that such polarization changes are characteristic of overpressured reservoirs. Similar large time-delays and polarization changes have been observed previously in an overpressured reservoir (Crampin *et al.* 1996; Slater 1997), and in the fault gouge of the San Andreas Fault where high pore-fluid pressures are expected (Liu *et al.* 1997).

3 DATA PROCESSING

The main issues in 4-D multicomponent data processing are to create high-resolution data with maximum repeatability and in this case the

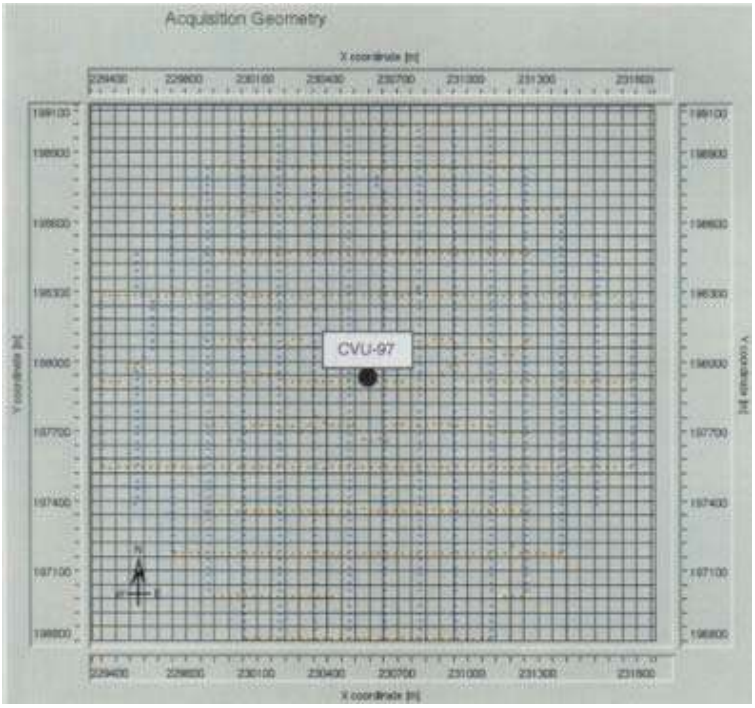

Figure 1. Acquisition geometry of Vacuum Field, sources run E–W and 3C receivers N–S. CVU-97 in the centre of the circular spread survey was used as the pilot CO_2 injection well in 1995.

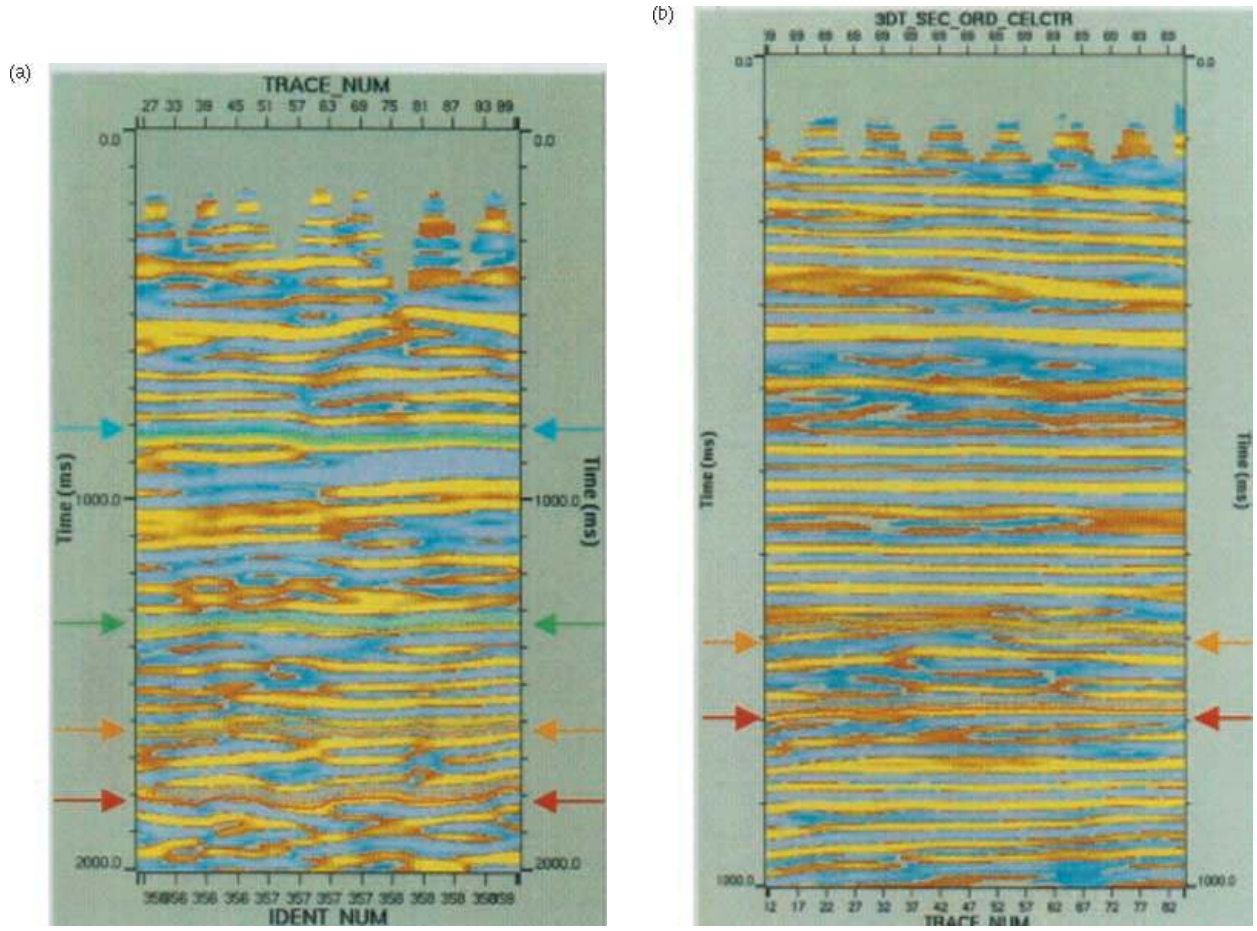

Figure 2. (a) Shear (*S1*) and (b) *P*-wave sections, orientated S to N, with picked horizons, base near-surface: blue; base salt: green; top San Andres: orange; base San Andres: red.

Table 1. Shear- and *P*-wave processing flows.

Shear-wave processing flow	*P*-wave processing flow
Surface statics	Surface statics
Alford rotation	
Surface-consistent deconvolution	Surface-consistent deconvolution
Trace edit	Trace edit
Surface-consistent amplitude corrections	Surface-consistent amplitude corrections
Outside mute	—
Velocity analysis and NMO correction	Velocity analysis and NMO correction
Residual statics	—
Stack	Stack
3-D random noise attenuation (RNA)	3-D random noise attenuation (RNA)
fk-dip filter	*fk*-dip filter
Bandpass filter	Bandpass filter
Residual amplitude analysis/ compensation	Residual amplitude analysis/ compensation
4-D matching filter	4-D matching filter

preservation of normal-incidence shear-wave anisotropy. Successful anisotropic processing needs to preserve the relative amplitudes between the components to preserve shear-wave polarization directions, and preserve the relative time-delays between shear-wave arrivals. A synthetic anisotropic seven-layer model based on the stratigraphic setting of the Vacuum Field was created to test the applicability of standard (*P*-wave) processing techniques to shear-wave data. The tested processing steps are deconvolution, dip filtering, stacking, random noise attenuation (RNA), which is a coherence filter in the *fx*-domain, and 4-D matching for time-lapse data. The criterion to evaluate the applicability is to determine the amount of change of the polarization directions and time-delays when applying the various processing techniques in the presence of noise. In the actual data processing, only parameters that were found to preserve normal incidence anisotropy were applied. Table 1 gives an overview of the shear- and *P*-wave processing sequences. From each multicomponent data set, we determine one *P*-wave data volume and four shear-wave data volumes (orthogonal *S1* and *S2* geophones recording two orthogonal shear-wave sources).

We use the surface statics correction, Alford rotation (Alford 1986), and surface-consistent deconvolution of Roche (1997). The maximum horizontal stress is in the N118°E direction, which we call the *S1*-direction, and the orthogonal N28°E, the *S2*-direction. The data are rotated into this natural coordinate system where the fast split shear-wave polarization is found to be parallel to the *S1* axis and the slow parallel to *S2*. Surface-consistent algorithms are used for both *P* waves and shear waves to increase repeatability as discussed by Lumley (1995). When using surface-consistent algorithms, amplitude scalars, deconvolution operators and static shifts are calculated for each source and receiver station. Every data trace has the operators of its corresponding source and receiver location applied. This is more stable than using operators that are calculated trace by trace and are therefore more sensitive to noise. The operators for surface-consistent amplitude correction and reflection statics were derived from the *S1* components and applied to all shear-wave components within each survey to preserve relative amplitudes and time-shifts. NMO corrections were then made on all components using a single 3-D velocity function picked from the *S1* data. Owing to noise problems a narrow mute was applied that only included data up to 800 m offset in the target zone. Post-stack noise attenuation procedures include 3-D RNA, two pass 2-D *fk*-filtering, and a bandpass filter. 3-D RNA is a multichannel *fx*-deconvolution process, where within time-windows the coherent signals of the data are predicted and the incoherent part, the random noise, is attenuated. A single variant gain function was derived from the combination of *S1* and *S2* components of each survey and applied to all four components to ensure the preservation of relative amplitudes. In the 4-D analysis, each trace of the first survey is matched to its equivalent trace in the second survey by a deconvolution process. Deconvolution operators, which are calculated on a trace by trace basis, compensate for wavelet and phase changes between the time-lapse surveys. The operators are estimated from time windows above the target as this is regarded as the repeatable part of a time-lapse survey. The *P*-wave processing flow is similar to the shear-wave flow. Surface-consistent parameters are derived for each data set individually. The same velocity function is applied to both data sets and the first survey is then matched to the second 4-D survey with better signal-to-noise characteristics.

4 DATA ANALYSIS

Fig. 2 shows shear-wave (*S1*) and *P*-wave record sections of the fully processed Phase VI data volumes with the interpreted horizons indicated. Roche (1997) identified the reflections by tying VSP data to the surface seismology. The sections can be roughly divided into three intervals. The top 850 ms in the shear-wave section (Fig. 2a) are near-surface sandstones and the reflections are cyclic and have high-frequency components. The interval between 850 and 1350 ms is a salt layer, where there are fewer reflections and the frequency content drops. This may be caused by greater homogeneity in the salt layer. Below the salt lies a sequence of dolomites that contains the target interval, the San Andres formation. The top (orange marker) following Roche (1997) lies around 1630 ms, the bottom is picked around 1820 ms (red marker). In the dolomites, cyclic reflections occur again, which indicates facies changes owing to cyclic sea level changes in deposition. In the shear-wave section, the target interval reflections are cyclic in the northern part and become less coherent in the south. In the *P*-wave section, the target is picked as a 100 ms interval lying between 680 ms and 780 ms. Cyclicity appears to be less a problem in *P* than it is in shear. Cyclic deposition can lead to tuning effects in the data, which may be either constructive or destructive interference of reflections from thin layers (Knapp 1990). This degrades resolution.

Anisotropic analysis is performed on the stacked data. The horizon picks provide interval traveltimes and time-delays of the split shear waves, which are used to calculate the percentage shear-wave velocity anisotropy as the normalized difference between the fast and the slow shear-wave velocities. *P*-wave interval time differences before and after injection are also calculated. Following Harris & Adler (1999), there is a shear-wave picking error of approximately 2.7 per cent and a *P*-wave picking error of 2 per cent. Nine-point median filtering was applied to the horizon picks, which reduces the error by a factor of $\sqrt{9}$ to 0.9 and 0.67 per cent for shear waves and *P* waves, respectively. In the difference sections, this error is multiplied by the square root of two which leads to total errors of 1.3 per cent for shear waves and 0.9 per cent for *P* waves. It is therefore possible to detect significant time-lapse changes. Fig. 3 shows the interval time analysis results before and after injection for shear and the interval time difference for *P* waves. Figs 3(a) and (b) are the percentage time delays between the *S1* and the *S2* shear-wave arrivals in the two surveys, and Fig. 3(c) is the percentage difference in shear-wave anisotropy before and after injection.

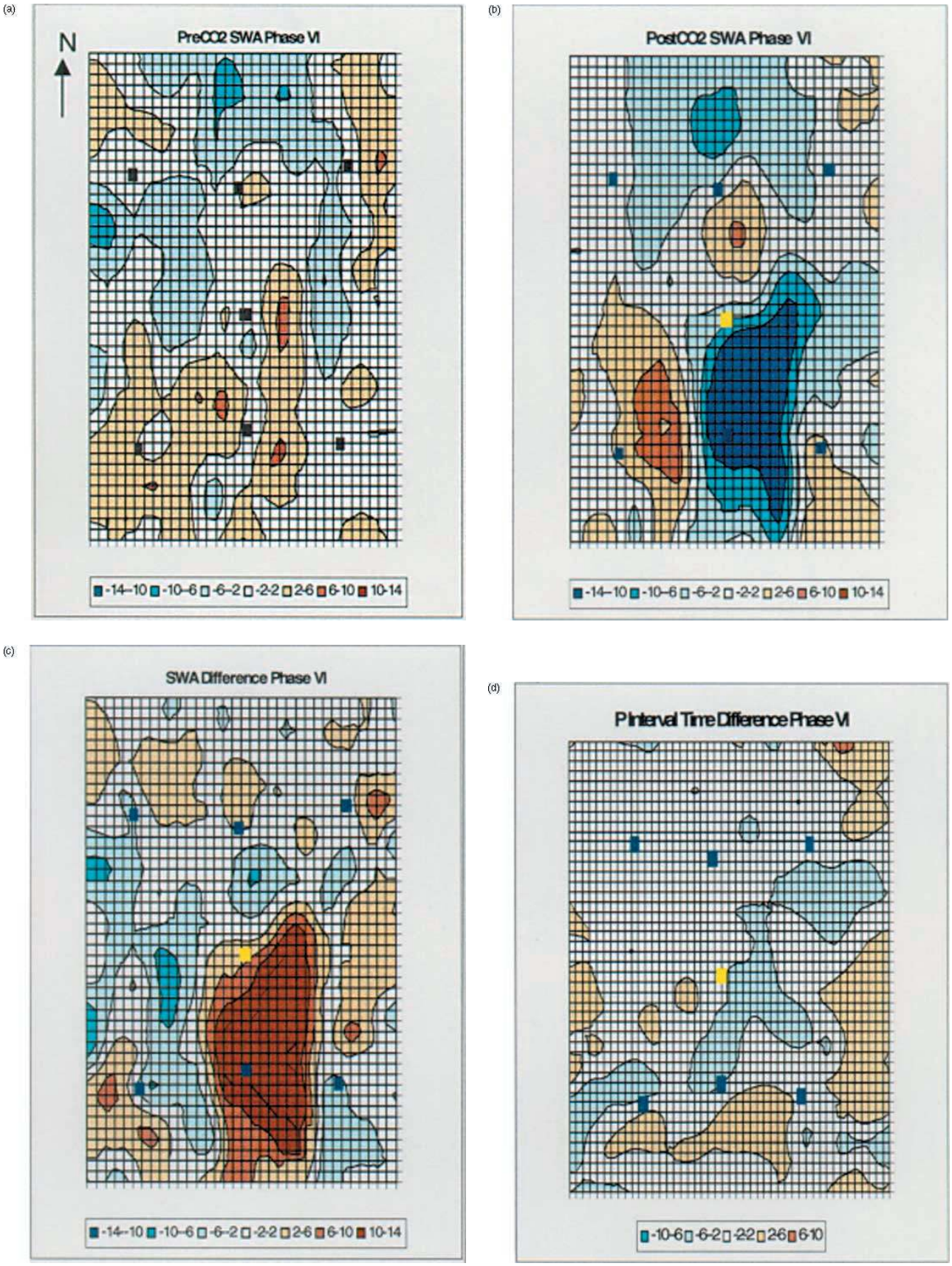

Figure 3. Shear-wave anisotropy of the San Andres interval of (a) the pre-CO_2, (b) the post-CO_2 survey, (c) the difference (pre-CO_2–post-CO_2); and (d) *P*-wave interval time difference. The values are in per cent. The wells are indicated and each gridpoint is one common midpoint (CMP). The distance between CMPs is 16.75 m.

Fig. 3(d) is the interval time-difference plot for *P* waves. Before the injection, the shear-wave time delays lie between ±2 per cent, which means shear-wave splitting is small but lies above the limits of resolution.

After the injection a zone with negative shear-wave splitting can be observed in Fig. 3(b) to the south and east of the injection well. The average value of anisotropy in the anomalous zone is −8 per cent. Peak values lie around −12 per cent. Both shear-wave arrivals are differentially later after the injection, where *S1* is relatively later than *S2*. This produces a 'negative anisotropy' where the shear-wave polarized parallel to the maximum horizontal stress direction is slower than the perpendicularly polarized wave. A similar observation of a negative anisotropy was made in an overpressurized reservoir by Crampin *et al.* (1996) based on the analysis of Slater (1997). The shear-wave difference plot, Fig. 3(c), shows that the injection caused a considerable increase in relative anisotropy of 10 per cent. The *P*-wave interval time difference plot, Fig. 3(d), also shows a zone of velocity decrease to the south and east of the injection well, with an average velocity change in this zone of 2 per cent with peak values of 5 per cent. The zone to the NW of the injection well shows very little changes in *P*-wave velocities. From the interval-time analysis it can be concluded that the combined effects of CO_2 injection and pore-fluid pressure increases are decreases in all body-wave velocities occurring mainly to the south and east of the injection well.

Polarization analysis was performed using the linear transform technique (Li & Crampin 1993). In the overburden above the target horizon, the polarization directions lie mostly within ±15° of the maximum horizontal stress direction, see Figs 4(a) and (b) for both surveys. It is probably owing to noise that the first (pre-CO_2) survey shows some areas with higher deviations of 15°–30°. In general, this result is a confirmation that the Alford rotation (Alford 1986) has been performed correctly. To evaluate the polarization directions of the target interval a layer stripping procedure was applied following an approach developed by Thomsen *et al.* (1995). The horizon picks of the top of the target provide the total time-delays between the fast and the slow shear waves that accumulate in the overburden, which are on average 12 ms. To strip off the overburden anisotropy of the overburden correctly, the total two-way time-delay is subtracted from the slow shear-wave component at each location and the one-way (half) time-delays are removed from the residual shear-wave components. Fig. 5 shows the resulting polarization directions of the target interval for the pre-CO_2 and the post-CO_2 surveys. To the NW, the polarization directions are in general more uniform and aligned parallel to the natural coordinate system. To the SE, the polarizations are very heterogeneous, especially in the pre-CO_2 survey. After injection there is better alignment in this quadrant. A possible explanation is that before the CO_2 injection the reservoir may have been in a heterogeneous condition as both production and water-injection processes had been in progress for decades. It is suggested that the significant pore-fluid pressure increase between the two surveys may have led to more homogeneously aligned polarization directions in the whole area. There is no significant polarization anomaly in the area of the identified time-delay changes. Cycle skipping effects may have introduced ambiguity in the measurements and so polarity reversals that follow from Fig. 3(b) cannot be verified.

5 MODELLING

In order to interpret and understand the observed time-lapse changes a 1-D model is matched to the data in the zone of the time-delay anomaly. The model incorporates both saturation and pressure changes. At first, the effects of a saturation change on the equant (non-aligned) porosity are investigated. It is assumed that such equant pores are distributed randomly and that the rock is isotropic. The CO_2 injection changes the density, compressibility and the viscosity of the reservoir fluid. Wang *et al.* (1998) made a rock physics study on the effects of CO_2 injection in a carbonate rock similar to the San Andres dolomite, and provide CO_2 density, bulk modulus, and compressional velocity as functions of pore-fluid pressure. The fluid bulk modulus of CO_2 is significantly lower than the bulk modulus of the reservoir fluid, by at least one order of magnitude: 0.2 and 0.25 GPa at pore-fluid pressures of 10.6 and 17 MPa, respectively, as opposed to 2.5 GPa for the bulk modulus of the reservoir fluid of oil with 38° API gravity and brine. Using Wood's equation (Batzle & Wang 1992), an average *P*-wave velocity of 780 m s^{-1} can be determined for a CO_2–oil–brine mixture. The fluid density is 1 g cm^{-3}, which is only slightly below the density of the original reservoir fluid of 1.06 g cm^{-3} (Roche 1997).

Endres & Knight (1997) derived a rock physics model that incorporates fluid-pressure communication into inclusion-based models, and so a single model can be used to calculate rock properties at both high and low frequencies. At low frequencies the results are equal to the Gassmann (1957) formulation so that the shear modulus is independent of fluid saturation. At low frequencies the pore-fluid pressures can equilibrate and the elastic moduli are smaller than at high frequencies. The required parameters of this model are the elastic moduli of the matrix (71 GPa for the bulk modulus and 31.5 GPa for the shear modulus), which consists of dolomite with up to 20 per cent anhydrite, a porosity of 12.7 per cent and the aspect-ratio spectrum of the pores. An aspect-ratio spectrum was derived so that the laboratory measurements of San Andres dolomite (Capello de Passalacqua 1995) and the observations in the seismic data can be matched. For the rock filled with reservoir fluid, this gave a bulk modulus of 43 GPa and a shear modulus of 23.7 GPa.

It is possible to calculate *P*- and shear-wave velocities of the San Andres formation for varying CO_2 content. Fig. 6 shows how *P*-wave and shear-wave velocities change when CO_2 is injected at 17 MPa pore-fluid pressure. The rock saturated with the reservoir fluid has a *P*-wave velocity of 5300 m s^{-1} and a shear-wave velocity of 2990 m s^{-1}. The *P*-wave velocity decreases with increasing CO_2 content, significantly for small amounts of CO_2, but with only a small variation for more than 20 per cent CO_2 saturation. As the shear modulus is constant, only the density causes changes in the shear-wave velocities, consequently, as the density decreases for increasing CO_2 content, the shear-wave velocities increase only slightly—less than 0.5 per cent at most, and on average 0.13 per cent at 17 MPa pore-fluid pressure. This change is too small to be resolved in surface seismic data. Fig. 6 shows that there are only minor changes to be expected owing to the change in saturation.

Note that Jack (1998) classifies dolomite as a hard rock that is generally not suitable for time-lapse seismic studies. When the porosity is low, the fluid contents have only a minor influence on the elastic moduli. The input isotropic *P*-wave velocities to the pressure modelling are 5300 m s^{-1} for the original saturation and 5240 m s^{-1} after CO_2 injection. The shear-wave velocity remains practically constant at 2990 m s^{-1} and the density is 2.65 g cm^{-3}. An overview of the rock parameters before and after CO_2 injection is given in Table 2. The elastic constants for these two isotropic, fluid-saturated rocks form the input for APE modelling where the effects of pressure changes are investigated and combined with the saturation changes.

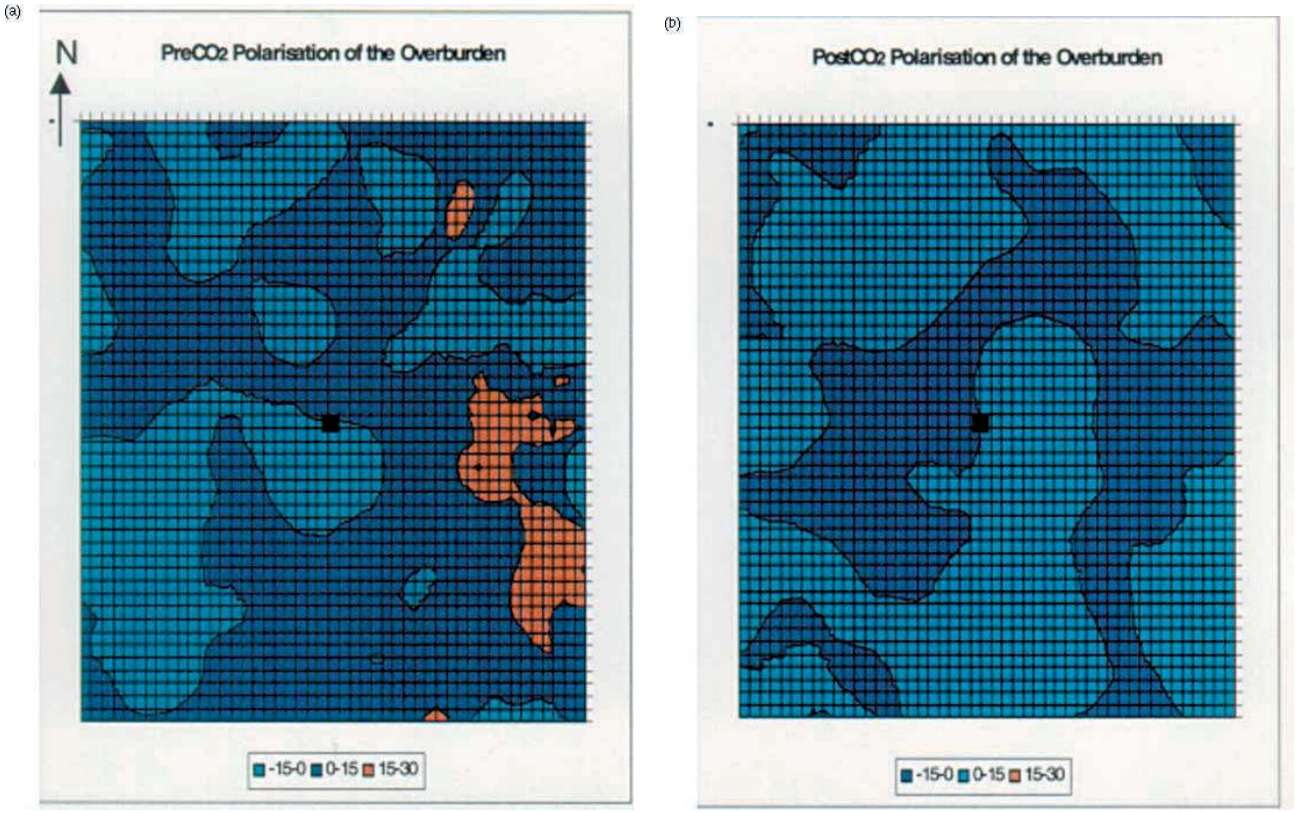

Figure 4. Polarization directions of the overburden for (a) the pre-CO_2 and (b) the post-CO_2 surveys. Directions are in degrees and relative to the natural coordinate system 118°–28°. The injection well is indicated and each gridpoint is one CMP location.

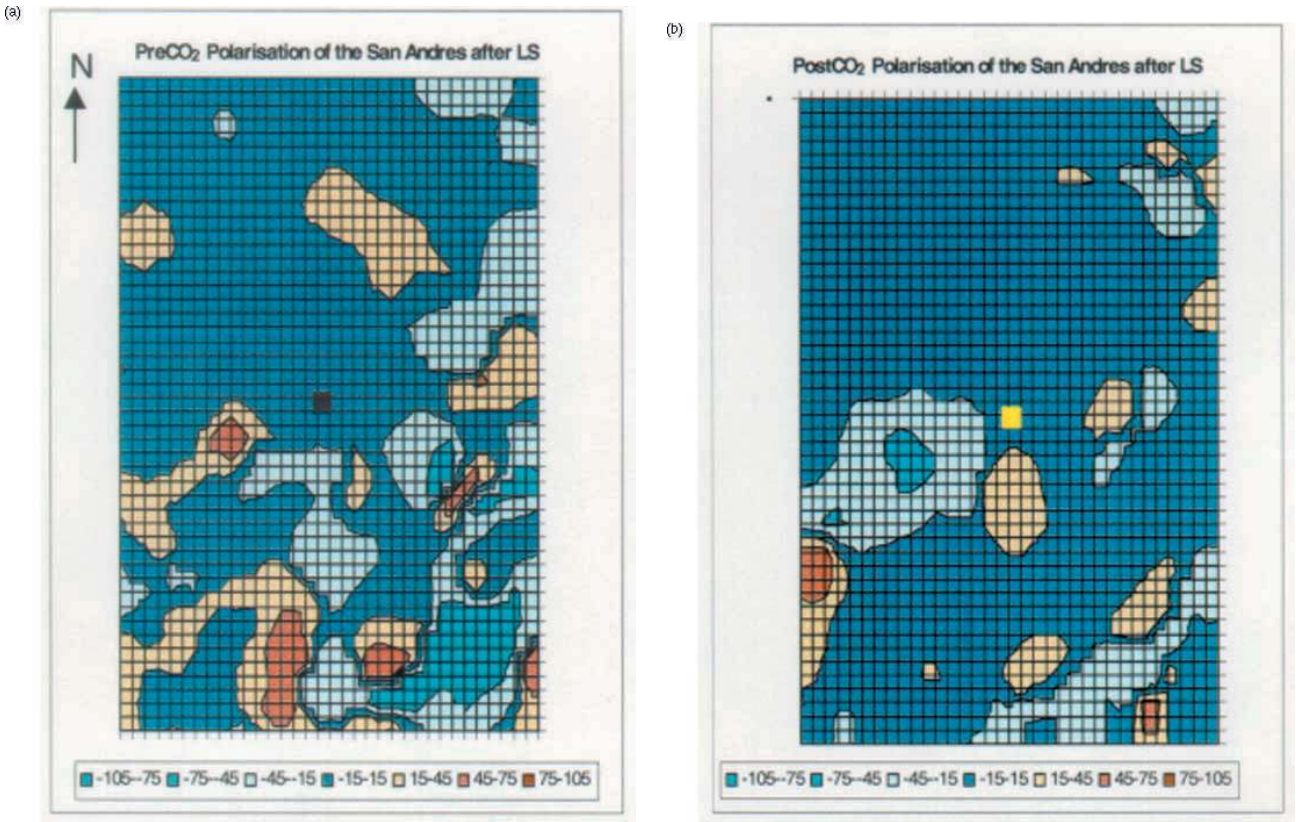

Figure 5. Polarization directions of the San Andres interval after layer stripping for (a) the pre-CO_2 and (b) the post-CO_2 surveys. Values are in degrees and relative to the natural coordinate system 118°–28°.

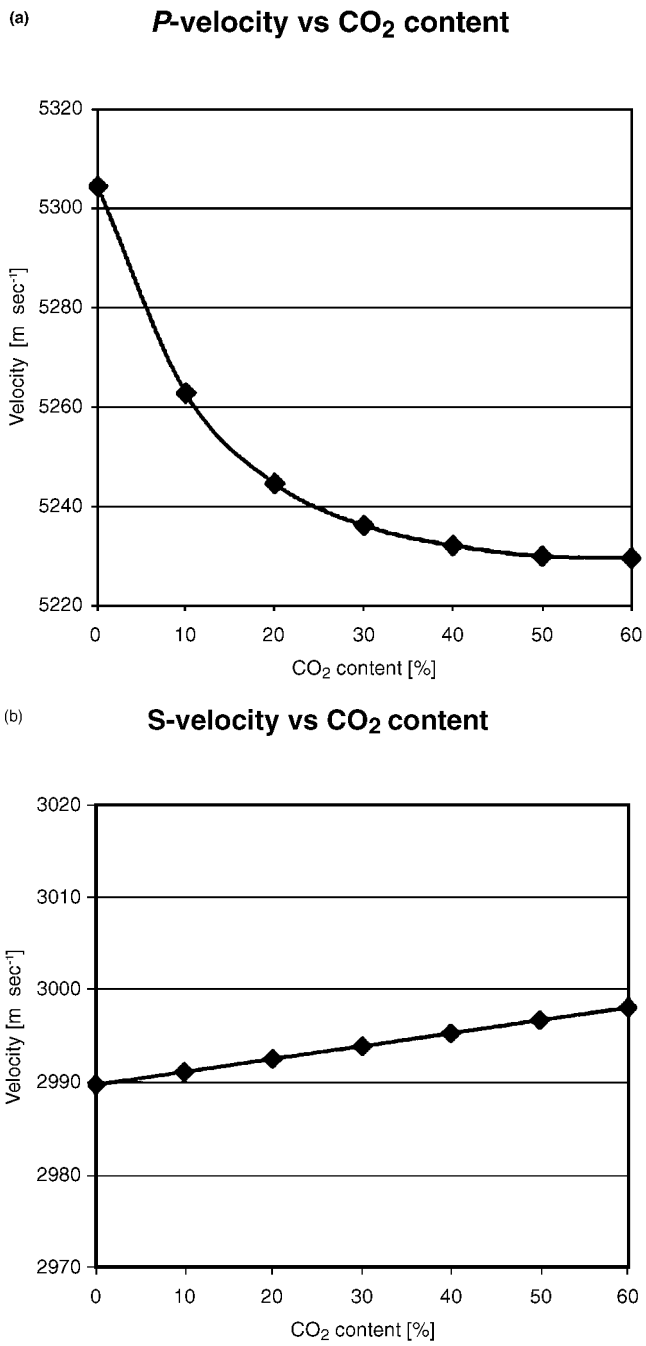

Figure 6. (a) *P*- and (b) *S*-wave velocities of the San Andres formation for varying CO_2 content and for two pore-fluid pressures.

The model does not include cracks with very low aspect ratios of less than 0.001. The reason for this is that these very thin cracks determine the soft or compliant porosity and respond to pressure changes. They are not randomly distributed in the presence of differential stresses, but tend to be aligned perpendicular to the minimum stress direction, and are the cause for the observed shear-wave splitting. The pore-fluid change in these compliant cracks is incorporated in APE modelling.

The parameters for APE modelling are five pressures, the crack geometry of the formation in an unstressed condition and pore-fluid parameters. These (average) pressures are the vertical overburden pressure, the minimum horizontal stress, the maximum horizontal stress, the pore-fluid pressure and the critical stress that is needed to close a small aspect-ratio crack. The pore-fluid pressure of the target zone, provided by Roche (1997), is the only pressure variable of the APE model that changes during the injection process. The pore-fluid pressure increased significantly from a 'normal' pressure of 10.6 MPa to an 'overpressure' of 17 MPa during the CO_2 injection and before production resumed when the second survey was acquired. The overburden pressure is 30 MPa. With these three pressures given, the other pressure parameters were tested to match the observed anisotropy change. Only for maximum horizontal stress values of 16–18 MPa, close to the pore-fluid pressure of 17 MPa, and minimum horizontal stresses from 0 to 5 MPa can suitable models be created. The critical stress is held constant at 1 MPa. The aspect ratios that fit the data range from 0.000 01 to 0.001. This is a very wide range and shows that at 0° incidence shear-wave splitting is not particularly sensitive to aspect ratios. The resulting *P*-wave and shear-wave velocities of the model incorporating saturation and pressure changes are summarized in Table 3 for normal incidence rays.

Table 2. Overview of changes in the isotropic reservoir rock properties of the San Andres formation when CO_2 is injected (Phase VI).

Rock property	Reservoir rock	
	Original at 10.6 MPa	Injected CO_2 at 17 MPa
Fluid density (g cm^{-3})	1.06	1
Rock density (g cm^{-3})	2.65	2.64
Fluid bulk modulus (GPa)	2.5	0.6
Rock bulk modulus (GPa)	43	41
Rock shear modulus (GPa)	23.7	23.7
P-wave velocity (m s^{-1})	5300	5240
S-wave velocity (m s^{-1})	2990	2995

The distribution of cracks in an unstressed state, or the total number of existing cracks, was derived from a shear-wave coherence analysis of the reservoir interval (Talley 1997), see Fig. 7. To the south of the injection well there are two zones of low coherence, which are interpreted as NS and N60°E trending faults. The faults correlate with the shear-wave velocity difference in Fig. 3(c). Fault-related, vertical cracks are therefore introduced into the APE model. The cracks are scattered within ±10° of the given directions. This range agrees with field observations of fault-related crack distributions (Anders & Wiltschko 1994) that normally range between ±(5°–20°) of the fault direction. In the 1980s, well CVU-97 had also undergone several stages of acid injection. This may have created additional fractures in the vicinity of the well with a possible preferential alignment parallel to existing faults. Acid fractures can be reopened whenever the pore-fluid pressure is higher than the pressure at the time of the acid injection. Before the CO_2 injection, these fault-related cracks are closed but are opened by the high-pressure injection. The modelled total fault-related crack densities of each set lies between 0.047 and 0.065. In addition to the two sets of fault-related cracks, 4 per cent randomly oriented cracks were

Table 3. Calculated body-wave velocities for the reservoir incorporating saturation and pressure changes.

Pore-fluid pressure (MPa)	v_{S1} (m s^{-1})	v_{S2} (m s^{-1})	v_P (m s^{-1})	SWVA (per cent)
10.6	2955	2915	5285	1.3
17	2485	2785	5108	−10.7

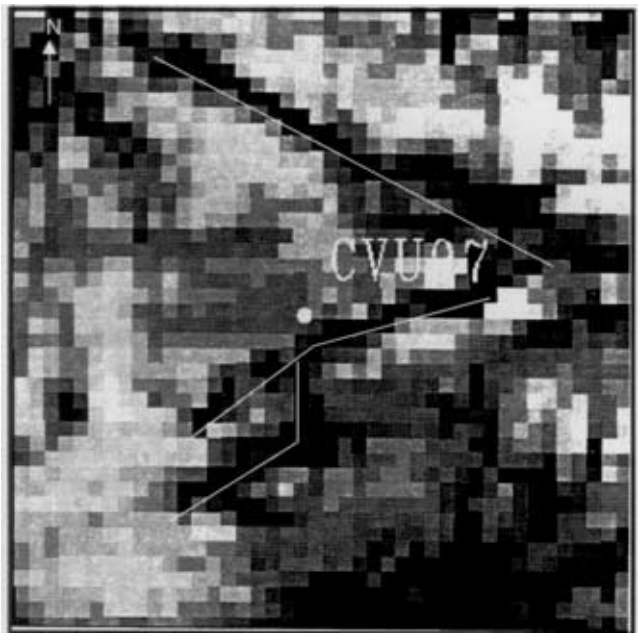

Figure 7. Shear-wave coherence analysis map of the San Andres interval (Talley 1997). Zones of low coherence appear in black and faults are interpreted. To the south of CVU-97 faults with NS and N60°E occur. The distance between CMP locations is 16.75 m.

modelled. The resulting model is a symmetric orthorhombic solution with equal crack densities for each fault and equal separation from the minimum stress direction. We also found a wide range of asymmetric solutions, which are not thought to be relevant, and are not discussed here.

Fig. 8 represents a horizontal section of a 2-D visualization of the direction and number of open cracks for both pore-fluid pressures. The APE model is 3-D, but nevertheless these simple 2-D plots are reasonably realistic as most of the open cracks are close to vertical. The vertical stress is the maximum stress and therefore cracks with incidence angles of up to 60° with respect to the vertical are closed throughout. Before injection, only random cracks subparallel to the maximum horizontal stress of 118° are open and the anisotropy is therefore positive. After the injection and a significant pore-fluid pressure increase of 6.4 MPa, previously closed cracks now open in all azimuths. This causes body-wave velocities to decrease and the *S1* component, which is parallel to 118°, is strongly affected as it decreases from 2955 m s^{-1} to about 2485 m s^{-1}, which is a 16 per cent velocity decrease. The *S2* component decreases about

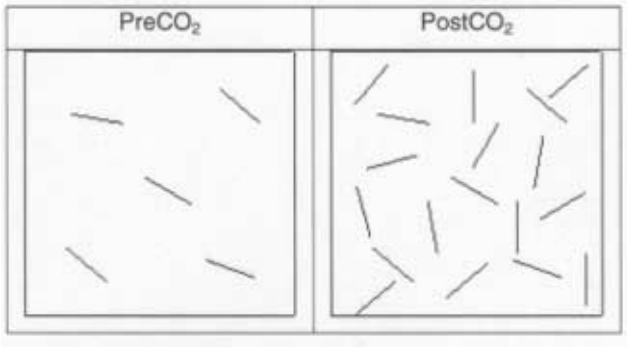

Figure 8. Simplified 2-D model of the number and orientation of open cracks before and after CO_2 injection.

4.5 per cent from 2915 to 2785 m s^{-1} and becomes the fast shear wave. If the pore-fluid remains the same, the *P*-wave velocity also marginally decreases, owing to the pressure increase from 5285 to 5205 m s^{-1} or 5108 m s^{-1}, with and without the saturation change considered. As the cracks are nearly vertical, the maximum effect for the *P* waves is expected at high, near-horizontal angles of incidence. Table 3 summarizes the resulting velocities of the APE and saturation model.

Synthetic seismograms for this model were calculated using ANISEIS (Taylor 2000) and are matched to the shear-wave data in Fig. 9. The model matches the data when the calculated shear-wave velocities are within ±30 m s^{-1} of the velocities determined in the analysis. For the *P* waves the range is about ±50 m s^{-1}. Both overburden and target are modelled by APE. Four reflections are matched, the bottom of the near-surface, the base of the salt, the top of the San Andres, and the base of the San Andres formation. Interval times are shown for the San Andres layer. This model gives a very good match for all components in the target formation as well as the overburden. The increase in pore-fluid pressure and the resulting differential opening of cracks adequately explain the observed interval time changes in the shear-wave sections. The amplitudes also match well for most of the reflections. This match between the data and the model shows that APE can be used to predict the stress-sensitive behaviour of shear-wave velocities in hydrocarbon reservoirs. That is APE predicts the response of the fluid-saturated rocks to changes of pore-fluid pressure. The APE model also matches the *P*-wave data. In the saturation modelling, the *P*-wave velocity of 5300 m s^{-1} was calculated for the isotropic rock saturated with the formation fluid and a velocity of 5240 m s^{-1} after CO_2 injection. Introducing the small aspect-ratio cracks reduces the velocity to 5285 m s^{-1} for a pore-fluid pressure of 10.6 MPa and to 5108 m s^{-1} at 17 MPa at normal incidence and after the CO_2 injection. The total modelled *P*-wave velocity decrease is therefore 3.3 per cent. It is possible to split the velocity decrease into a pressure component and a component that reflects the pore-fluid compressibility change. The pressure effect is therefore $5285 - 5205 = 80$ m s^{-1} or 1.5 per cent. When CO_2 is injected the velocity decreases $5205 - 5108 = 97$ m s^{-1} or 1.8 per cent. For normal incidence *P* waves, the effect of the saturation change is larger than the pressure change. From the horizon picks interval times of 97 and 100 ms result for the pre- and post-CO_2 surveys. This is less than two samples difference and lies within the picking error of 4 per cent and does not create a significant time-lapse effect. Fig. 10 depicts the fit of the *P*-wave synthetics to the observed data. The model is a good fit both in reflection times and amplitudes for all six layers. The top of the San Andres is a weak trough. The amplitude of the bottom target reflection is well defined and increases after the injection, as the impedance contrast increases owing to the velocity decrease in the target. In the overburden, the top of the salt is a much stronger reflection at 330 ms than the top salt in shear-wave section at around 1000 ms. In general, the reflection character is very similar in both *P*-wave sections. This again indicates good repeatability and shows that the CO_2 injection has little effect on the overburden.

6 PHASE VII

In 1998 a second, more widespread CO_2 injection programme took place in Vacuum Field. Two more time-lapse surveys, one before, and one during the injection were acquired. Variations in the shear-wave source pattern prevent a complete integration of Phases VI and VII into a single project. After processing and analysing the data following the method described here, the APE model that

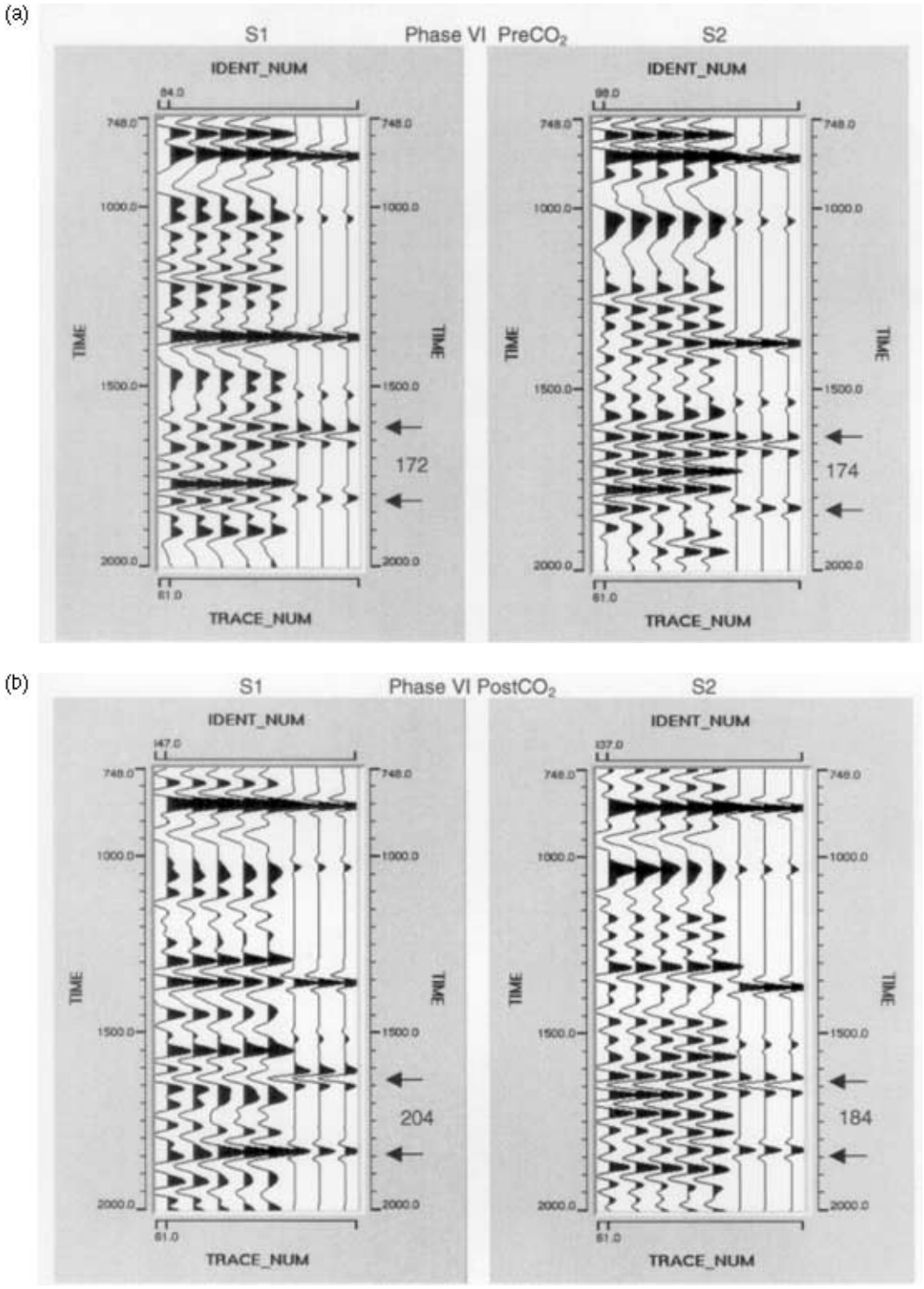

Figure 9. Match between stacked shear-wave data (the first five traces of each panel) and the synthetic (the remaining three traces of each panel) for the San Andres formation and the overburden in the zone of the time-delay anomaly. The interval times in the San Andres are indicated.

had been established for the Phase VI data also matched Phase VII data at the chosen location. A small pore-fluid pressure increase of 1.4 MPa was estimated during the injection. (Note that this was not enough to cause an overpressure and consequently did not change the shear-wave polarizations.) The fit of the synthetic data to the real data is shown in Fig. 11 for the shear waves and in Fig. 12 for the *P* waves. The *S1* velocity change is below resolution. The *S2* and *P*-wave velocities decrease less than 2 per cent. The polarization directions of the shear waves remain unchanged as the pore-fluid pressure increases were below overpressures. This example shows that it is possible to predict the response of a fractured, fluid-filled rock to subsurface stress and pressure changes. It is also possible to calculate the seismic response, once a well-calibrated APE model has been established for the particular location.

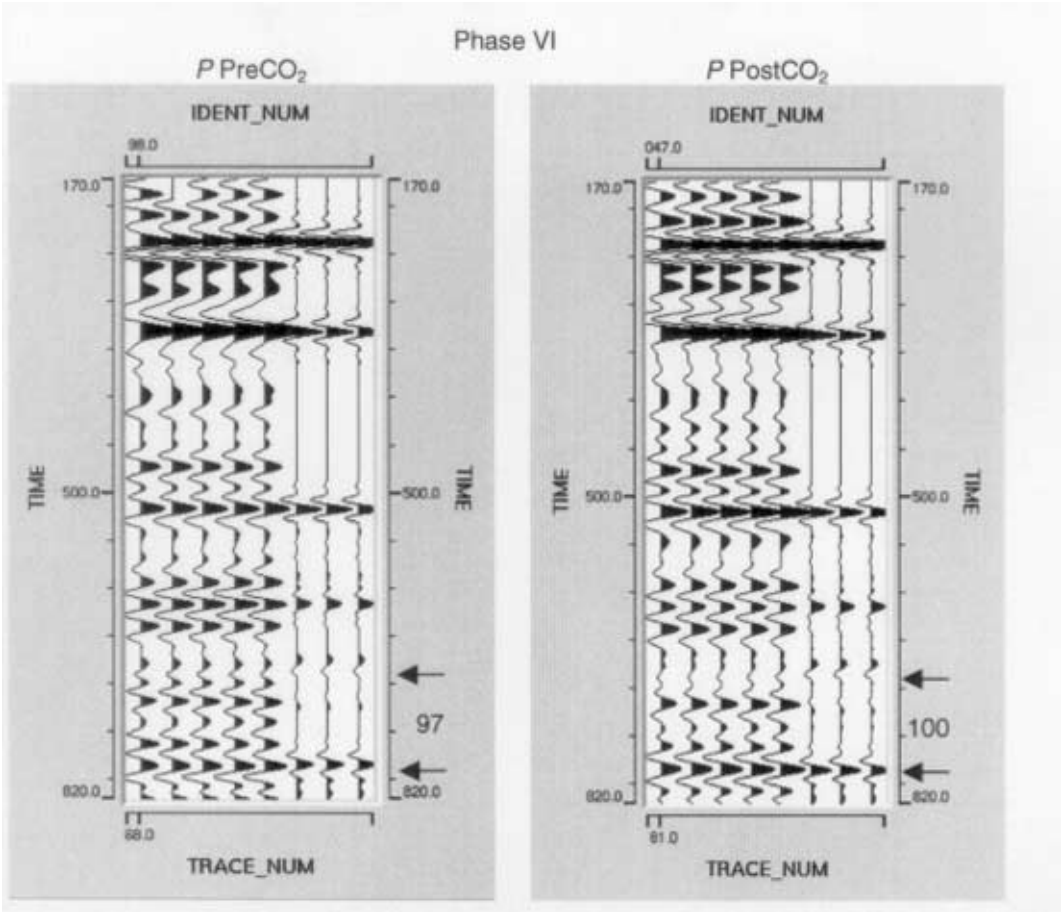

Figure 10. Match between stacked *P*-wave data (the first five traces of each panel) and the synthetic (the remaining three traces of each panel) for the San Andres formation and the overburden in the zone of the time-delay anomaly. The interval times in the San Andres are indicated.

7 CONCLUSIONS

This paper reports an applied reservoir study where time-lapse multicomponent seismic data are processed, analysed, interpreted, modelled and *the response for known fluid-injection pressures predicted*, in an integrated fluid monitoring exercise. Despite the limitations in data quality this study identifies significant time-lapse velocity effects in normal-incidence waves leading to changes in shear-wave velocity anisotropy. Although the reservoir rock in Vacuum Field, the San Andres dolomite, is a comparatively hard rock, time-lapse effects occur, due to pressure-dependent changes in crack aspect ratios as injection modifies pore-fluid pressures, and to 90°-flips in shear-wave polarizations when overpressures are induced.

Synthetic seismograms based on poro-elastic models, developed by Endres & Knight (1997) and Zatsepin & Crampin (1997), that incorporate saturation and pressure changes are successfully matched with the real data in the vicinity of the central well CVU-97 before and after the injected changes. The effect of changing saturation is a 1.8 per cent velocity decrease in *P*-wave velocity but with no change in shear-wave velocity. The effect of the high injected pressure is a further 1.5 per cent decrease in *P*-wave velocity, and very significant changes in shear-wave velocity anisotropy due entirely to the pore-fluid pressure increasing crack aspect ratios. With this model it is possible to predict the seismic response of hydrocarbon production operations, and this procedure is the first really comprehensive calibration of *in situ* APE modelling.

Observations

There are three main observations for the Phase VI data set. (The Phase VII data set gives low-pressure results, compatible with Phase VI, but is not described in detail here.)

(1) The absolute value of shear-wave velocity anisotropy changes from an average of 2.2 per cent, to −8 per cent after high-pressure CO_2 injection in the reservoir to the S and SE of the injection well, where the negative anisotropy represents a change in the polarization of the faster split shear wave. This zone correlates with zones of low seismic coherence, indicating the presence of aligned faults and fractures.

(2) After CO_2 injection the shear-wave polarities are interchanged as the shear wave parallel to the maximum stress direction becomes the slow wave and the shear wave perpendicular to the maximum stress becomes the fast wave.

(3) Near-vertical *P*-wave velocities also decrease on injection by 3 per cent, which is about one-third decreasing the shear-wave velocities.

Main conclusions

(1) The pore-fluid pressure increases cause the differential opening of cracks and low-aspect-ratio pores, which leads to decreases in all body-wave velocities. The shear-wave velocities decrease differentially and a significant variation in the degree of shear-wave velocity anisotropy is observed.

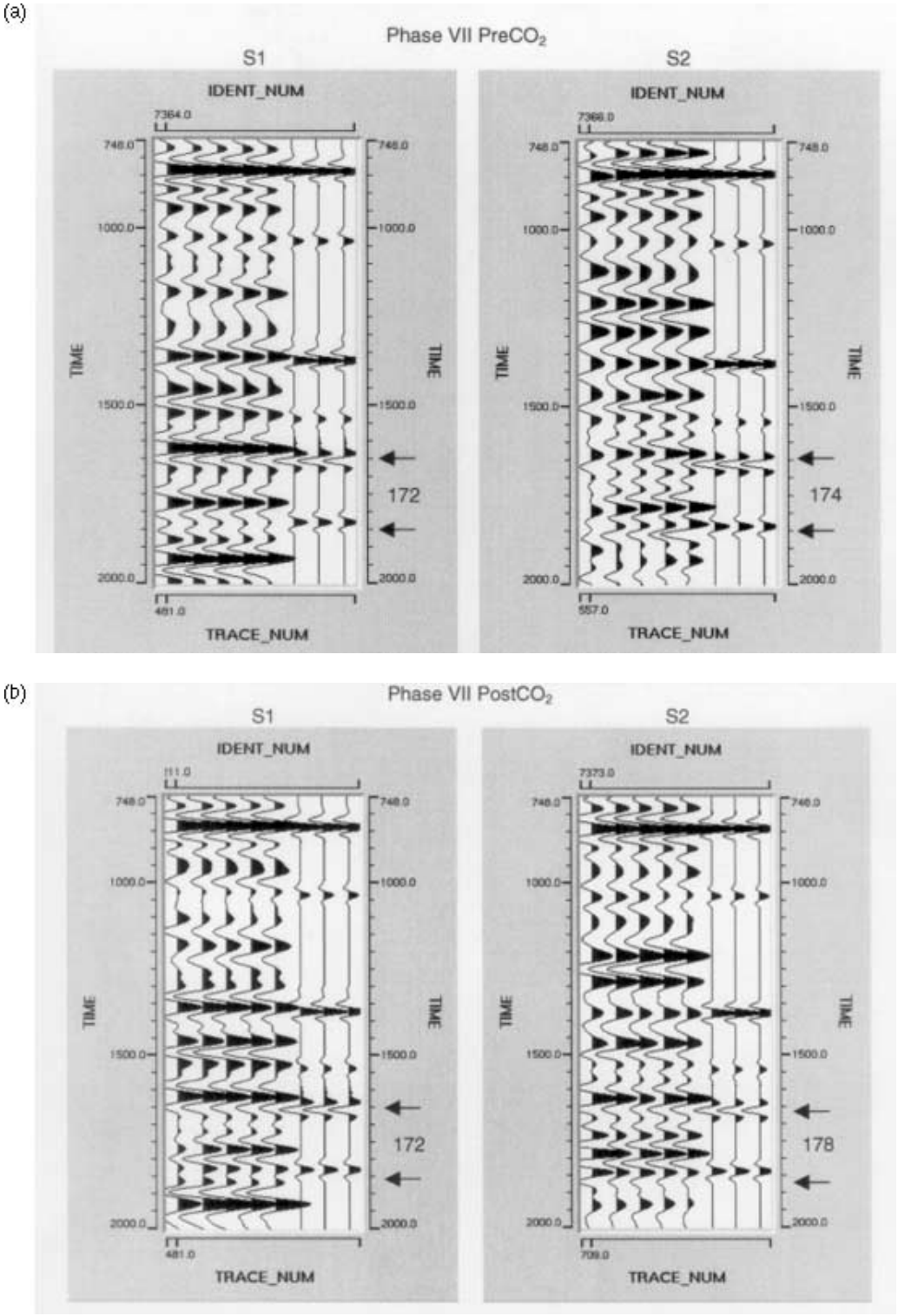

Figure 11. Match between stacked shear-wave data and APE model for the Phase VII data. The interval times in the San Andres are indicated.

(2) The saturation change caused by injecting CO_2 into the reservoir interval has little effect on the effective elastic properties of the fluid-filled material, even though the compressibility of the CO_2 is an order of magnitude smaller than the compressibility of the reservoir fluid.

(3) The principal effect of pressure changes is the preferential opening and closing of cracks, hence changes from finite to vanishing aspect ratios and vice versa, which causes a change in alignment and thus anisotropy.

(4) We suggest that it could not be expected from classical approaches that the detailed response of reservoir rock to two known fluid-injection pressures could be calculated (predicted) by anisotropic poro-elasticity modelling. This behaviour is believed to be caused by the critical nature of the crack distributions in the crust

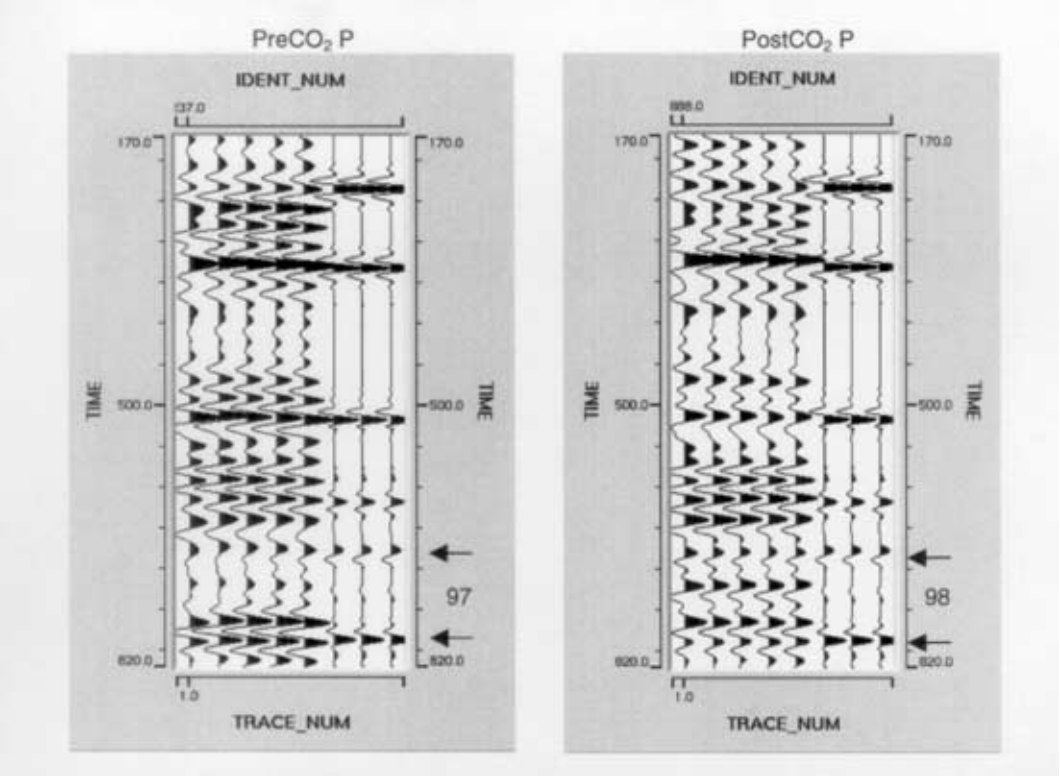

Figure 12. Match between stacked *P*-wave data and APE model for the Phase VII data. The interval times in the San Andres are indicated.

as discussed in the Appendix. The Appendix suggests that the crust as a critical system has profound implications for many standard reservoir characterization procedures.

ACKNOWLEDGMENTS

The authors would like to thank the Reservoir Characterization Project, Colorado School of Mines, for their co-operation and for providing the seismic data. We thank Macroc Ltd for providing the ANISEIS program. Erika Angerer was sponsored by WesternGeco. We are very grateful to Sven Treitel and John Dillon, who reviewed the paper, and also to Leon Thomsen for their comments and suggestions that helped to improve the paper. The work of Stuart Crampin was partially supported by European Commission Contract No. EVR-CT1999-40002.

REFERENCES

Alford, R.M., 1986. Shear data in the presence of azimuthal anisotropy, *SEG Expanded Abstracts,* 476–479.

Anders, M.H. & Wiltschko, D.V., 1994. Microfracturing palaeostress, and the growth of faults, *J. Struct. Geology,* **16,** 795–815.

Angerer, E., Crampin, S. & Li, X.-Y., 2000a. Changes in shear wave anisotropy in time-lapse data: a case study, *62nd Conf. EAGE, Glasgow, Extended Abstracts,* **1,** X-38.

Angerer, E., Crampin, S., Li, X.-Y. & Davis, T.L., 2000. Time-lapse seismic changes in a CO_2 injection process in a fractured reservoir, *70th Ann. Int. SEG Mtg., Calgary,* **2,** 1532–1535.

Batzle, M. & Wang, Z., 1992. Seismic properties of pore fluids, *Geophysics,* **57,** 1396–1408.

Bruce, A. & Wallace, D., 1989. Critical point phenomena: universal physics at large length scale, in *The New Physics,* pp. 236–267, ed. Davis, P., Cambridge University Press, Cambridge.

Capello de Passalacqua, M., 1995. Geology and rock physics of the San Andres formation in Vacuum Field, New Mexico, *MSc Dissertation,* Colorado School of Mines.

Crampin, S., 1994. The fracture criticality of crustal rocks, *Geophys. J. Int.,* **118,** 428–438.

Crampin, S., 1998. Shear-wave splitting in a critical crust: the next step, in *Proc. 8th Int. Workshop on Seismic Anisotropy, Boussens, 1998, Rev. Inst. Franc. Pet.,* **53,** 749–763, ed. Rasolofosaon, P.

Crampin, S., 1999. Calculable fluid-rock interactions, *J. geol. Soc.,* **156,** 501–514.

Crampin, S. & Chastin, S., 2000. Shear-wave splitting in a critical crust: II—compliant, calculable, controllable fluid-rock interactions, in *Anisotropy 2000, Fractures converted waves and case studies, Proc. 9th Int. Workshop on Seismic Anisotropy, Cape Allen 2000,* eds Ikelle, L.T. & Gangi, T.

Crampin, S. & Zatsepin, S.V., 1997. Modelling the compliance of crustal-rock, II—response to temporal changes before earthquakes, *Geophys. J. Int.,* **129,** 495–506.

Crampin, S., Zatsepin, S.V., Slater, C. & Brodov, L.Y., 1996. Abnormal shear-wave polarizations as indicators of pressures and over pressures, *58th Conf. EAGE, Amsterdam, Extended Abstracts,* X038.

Crampin, S., Volti, T. & Stefánsson, R., 1999. A successfully stress-forecast earthquake, *Geophys, J. Int.,* **138,** F1–F5.

Davis, T.L., Benson, R.D., Roche, S.L. & Talley, D., 1997. 4-D 3-C seismology and dynamic reservoir characterization—a geophysical renaissance, *67th Ann. Int. SEG Meeting, Dallas, Expanded Abstracts 1997,* **1,** 880–882; see also 883–885 and 886–889.

Duerrast, H. & Siegesmund, S., 1999. Correlation between rock fabrics andphysical properties of carbonate rocks, *Int. J. Earth Sci.,* **88,** 392–408.

Endres, A.L. & Knight, R.J., 1997. Incorporating pore geometry and fluid pressure communication into modelling the elastic behaviour of porous-rocks, *Geophysics,* **62,** 106–117.

Gaiser, J.E., 1999. Applications for vector coordinate systems of 3-D converted wave data.

Gassmann, F., 1957. Über die Elastizität poröser Medien, *Z. Naturf.,* **96,** 1–24.

Jack, I., 1998. Time-lapse seismic in reservoir management, *1998 SEG Distinguished Instructor Short Course.*

Jensen, H.J., 1998. *Self-organised Criticality,* Cambridge University Press, Cambridge.

Harris, P.E. & Adler, F., 1999. Seismic resolution and uncertainty intimelapse studies, *SEG Expanded Abstracts,* 1671–1674.

Knapp, J., 1990. Vertical Resolution of thick beds, thin beds, and thin-bed cyclothems, *Geophysics,* **55,** 1183–1190.

Li, X.-Y. & Crampin, S., 1993. Linear-transform techniques for processing shear-wave anisotropy in four-component seismic data, *Geophysics,* **58,** 240–256.

Liu, Y., Crampin, S. & Main, I., 1997. Shear-wave anisotropy: spatial and temporal variations in time delays at Parkfield, Central California, *Geophys. J. Int.,* **130,** 771–785.

Lumley, D., 1995. Seismic time-lapse monitoring of subsurface fluid flow, *PhD dissertation,* Stanford University.

Ma, S., 1976. *Modern Theory of Critical Phenomena, Frontiers in Physics,* Benjamin-Cummings, Reading, MA.

Rai, C.S. & Hanson, K.E., 1988. Shear-wave velocity anisotropy in sedimentary rocks: a laboratory study, *Geophysics,* **53,** 800–806.

Roche, S.L., 1997. Time-lapse, multicomponent, three-dimensional seismic-characterization of a san andres shallow shelf carbonate reservoir, vacuumfield, Lea County, New Mexico, *PhD Dissertation,* Colorado School of Mines.

Roche, S.L., Davis, T.L. & Benson, R.D., 1997. 4-D, 3-C seismic study at Vacuum field, New Mexico, *SEG Expanded Abstracts,* 886–889.

Scuta, M.S., 1997. 3D-reservoir characterization of the central vacuum unit, Lea County, New Mexico. *PhD Dissertation,* Colorado School of Mines.

Slater, C.P., 1997. Estimating and modelling of anisotropyin vertical andwalkaway seismic profiles at two North Caucasus Oil Fields, *PhD Dissertation,* University of Edinburgh.

Talley, D.J., 1997. Characterization of a San Andres carbonate reservoirusing four dimensional, multicomponent attribute analysis, *MSc Dissertation,* Colorado School of Mines.

Taylor, D.B., 2000. Manual: Version 5.5 Macroc Ltd, 31 Palmerston Place, Edinburgh.

Thomsen, L., Tsvankin, I. & Mueller, M.C., 1995. Layer-stripping of azimuthal anisotropy from reflection shear-wave data, *SEG Expanded Abstracts,* 289–292.

Wang, Z., Cates, M.E. & Langan, R.T., 1998. Seismic monitoring of a CO_2 flood in a carbonate reservoir: a rock physics study, *Geophysics,* **63,** 1604–1617.

Winterstein, D.F. & Meadows, M.A., 1991. Shear-wave polarisation and subsurface stress directions at Lost Hill Field, *Geophysics,* **56,** 1331–1348.

Zatsepin, S.V. & Crampin, S., 1997. Modelling the compliance of crustal rock—I. Response of shear-wave splitting to differential stress, *Geophys. J. Int.,* **129,** 477–494.

APPENDIX: THE CRACKED CRUST AS A CRITICAL SYSTEM

We briefly review the suggestions of Crampin (1998) and Crampin & Chastin (2000) that several types of behaviour in crustal rocks are inexplicable by conventional approaches. These include: nearly universal observations of stress-aligned shear-wave splitting in almost all *in situ* rocks; self-similar distributions of cracks and microcracks and the well-known Gutenberg–Richter relationship; self-similarity of $1/f$-noise of well-log spectra; and the occurrence of earthquakes, where critical phenomena are usually described by particular one-off explanations in terms of conventional geophysics. The surprising result of this paper that the fluid–rock interactions of specific fluid injections can be calculated (predicted) by APE modelling is a further result inexplicable by conventional approaches.

Crampin (1998) and Crampin & Chastin (2000) suggest that the reason for these conventionally inexplicable results are that the fluid-saturated crack distributions are critical systems. Critical systems are dynamic interactive non-linear systems that below criticality perturb only locally, whereas when systems reach criticality, individual members of the system may influence all other members over an extensive volume (Ma 1976). A critical system of cracks is a fundamental assumption for the development of APE modelling (Zatsepin & Crampin 1997). Crampin (1994) shows that observations of stress-aligned shear-wave splitting in the crust demonstrate that most ostensibly intact rocks below 1 km depth are verging on levels of fracture criticality when shear strength is lost and the percolation threshold exceeded (Crampin & Zatsepin 1997).

Bruce & Wallace (1989) show how different critical systems have remarkably similar statistical behaviour at criticality, despite very different subcritical physics. This is known as critical-point universality and implies self-similar scaling. This means that much of the behaviour of such critical systems is controlled by the behaviour close to criticality rather than by the classical physics of the subcritical matrix material. Crampin (1999) shows howdespite the complexity and heterogeneity of the Earth's crust, modelling with the highly constrained mean field theory (Jensen 1998) of APE matches the behaviour of distributions of fluid-saturated cracks, sometimes very accurately, over a wide range of different phenomena (Crampin & Chastin 2000).

Thus the reason for the remarkable predictability reported in this paper is believed to be that the response of such critical systems of cracks is controlled by the non-linear behaviour near criticality. Such criticality has serious implications for reservoir characterizationlisted in Table A1 (Crampin & Chastin 2000). Note that the limitationsin Table A1 are only valid if high-resolution detailed temporal and spatial measurements are required. If we are content with current comparatively coarse level of resolution is sufficient, then the restrictions in Table A1 may be ignored.

Table A1. Effects of critical systems of cracks on reservoir characterization.

1. Reservoir properties may change from place to place, even in supposedly homogeneous layers.
2. Reservoir properties may change with time, even without production processes.
3. Consequently, relevant properties need to be measured at the time and place they are required.
4. Response to known changes may in some circumstances be calculated (predicted) (Angerer *et al.* 2000a,b, this paper).
5. Response of reservoir may in some circumstances be controlled by monitoring the response to Item 4, above, by shear-wave splitting and adjusting changes to optimize the response.
6. There is the possibility of long-range and long-time correlation across reservoirs.
7. There is limit to the resolution of any measurement.